ACS APPLIED MATERIALS & INTERFACES

Research Article

www.acsami.org

Hierarchical Mn_2O_3 Hollow Microspheres as Anode Material of Lithium Ion Battery and Its Conversion Reaction Mechanism Investigated by XANES

Hang Su,[†] Yue-Feng Xu,[‡] Shan-Cheng Feng,[‡] Zhen-Guo Wu,[§] Xue-Ping Sun,[∥] Chong-Heng Shen,[‡] Jian-Qiang Wang,[∥] Jun-Tao Li,[†] Ling Huang,[‡] and Shi-Gang Sun*[,†,‡]

[†]College of Energy & School of Energy Research and [‡]College of Chemistry and Chemical Engineering, Xiamen University, Xiamen 361005, China

[§]School of Chemical Engineering, Sichuan University, Chengdu 610065, China

[∥]Shanghai Synchrotron Radiation Facility, Chinese Academy of Sciences, Shanghai 201204, China

Supporting Information

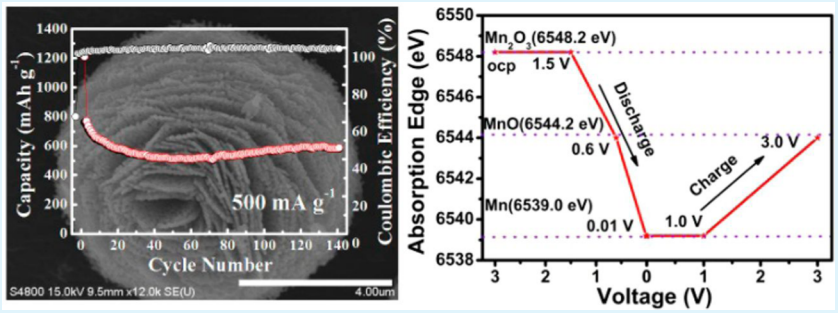

ABSTRACT: Hierarchical Mn_2O_3 hollow microspheres of diameter about 6−10 μm were synthesized by solvent-thermal method. When serving as anode materials of LIBs, the hierarchical Mn_2O_3 hollow microspheres could deliver a reversible capacity of 580 mAh g^{-1} at 500 mA g^{-1} after 140 cycles, and a specific capacity of 422 mAh g^{-1} at a current density as high as 1600 mA g^{-1}, demonstrating a good rate capability. Ex situ X-ray absorption near edge structure (XANES) spectrum reveals that, for the first time, the pristine Mn_2O_3 was reduced to metallic Mn when it discharged to 0.01 V, and oxidized to MnO as it charged to 3 V in the first cycle. Furthermore, the XANES data demonstrated also that the average valence of Mn in the sample at charged state has decreased slowly with cycling number, which signifies an incomplete lithiation process and interprets the capacity loss of the Mn_2O_3 during cycling.

KEYWORDS: *Mn_2O_3, hierarchical hollow microspheres, lithium ion battery, conversion reaction mechanism, XANES*

1. INTRODUCTION

Lithium ion batteries (LIBs) are widely used in mobile phones, portable electronic devices, and notebook computers.[1,2] However, since the graphite anode material of commercial LIBs is approaching its inherent limit in performance, the LIBs could hardly fulfill the growing demands of fast development of electric vehicles (EVs), hybrid EVs, and plug-in hybrid EVs in terms of energy density, power, and safety. Transition metal oxides such as iron oxide,[3,4] cobalt oxide,[5−7] nickel oxide,[8] and manganese oxide[9,10] have a higher energy density than graphite and have been widely studied as alternative anode materials of LIBs. Manganese oxides, as one kind of transition metal oxides, have a high theoretical specific capacity, can operate at a low conversion potential, and are abundant with low cost and environmental benignity. They are therefore appropriate for the electrode materials of LIBs.[11] Among the manganese oxides, Mn_2O_3 has a theoretical capacity as high as 1018 mAh g^{-1}, while it has a low electronic conductivity and poor cycle ability due to large volume expansion during charge−discharge, which hampered its application as anode in rechargeable LIBs.[12,13] Many studies have recently focused on the structure-controlled synthesis of Mn_2O_3 in order to enhance their electrochemical performances.[14] Hu et al. prepared Mn_2O_3 microspheres assembled from porous nanosheets.[15] The Mn_2O_3 microspheres could deliver a reversible capacity of 748 mAh g^{-1} at 50 mA g^{-1} over 45 cycles. Chen et al. synthesized Mn_2O_3 microstructured spheres and polyhedrons,[16] and demonstrated that the Mn_2O_3 samples could deliver a capacity of only 190 mAh g^{-1} after 15 cycles.

The cycle performance of the Mn_2O_3 electrodes is strongly related to the tremendous volume change in conversion reaction. One of the widely adopted strategies, in general, to

Received: December 30, 2014
Accepted: February 23, 2015
Published: February 23, 2015

DOI: 10.1021/am509198k
ACS Appl. Mater. Interfaces 2015, 7, 8488−8494

improve the cycling performance is to synthesize the Mn_2O_3 particles to the nanometer scale.[17−21] However, nanoparticles in electrodes easily self-aggregate under a relatively high current density owing to their high surface energy, which results in reducing the effective contact areas of electrode materials and electrolyte and leads consequently to gradual decrease in capacity.[22] To further improve the cycle performance of the transition metal oxide electrodes, hierarchical micro/nanostructure is regarded as an optimized design to keep the electrodes stable in charge/discharge processes,[23−25] because the hierarchical micro/nanostructure can inherit the advantages from both the nanoparticles and the microsized aggregation and offer thus a high structure stability in mechanical strength. Moreover, constructing the anode materials with hollow structure could be also an effective strategy to buffer the large volume variation.[26−29]

To the best of our knowledge, despite many efforts focusing on how to improve the electrochemical performance of Mn_2O_3 electrodes were reported, the conversion reaction mechanism of Mn_2O_3 electrodes has not been well-defined. Many results support that the conversion reaction of Mn_2O_3 electrodes undergoes a transformation between MnO_x ($0 < x < 1$) and Mn.[30−33] By analyzing the electrochemical results, on the contrary, Deng et al. speculated that porous Mn_2O_3 microspheres could be oxidized to Mn^{3+} after charging to 3 V.[34] It is still a challenge so far to make clear the conversion reaction mechanism and capacity fading of the Mn_2O_3 anode. X-ray absorption near edge structure (XANES) spectroscopy is an excellent technique to characterize the valence state of element in compounds,[35,36] and it was applied in this study to investigate the conversion reaction mechanism and the origin of capacity fading of Mn_2O_3 electrodes.

Some metal oxides anode materials of LIBs synthesized from metal-EG precursors have been reported lately.[15,37] The annealing of metal-EG precursors was demonstrated as an efficient method to obtain metal oxide materials with special morphology. In the current paper, hierarchical Mn_2O_3 hollow microspheres were synthesized by an improved solvent-thermal method using polyvinylpyrrolidone (PVP K-30) in the synthesis process and followed by calcination. The hierarchical Mn_2O_3 hollow microspheres could deliver a reversible capacity of 580 mAh g^{-1} at 500 mA g^{-1} after 140 cycles, and with a coulombic efficiency of 99.7%. A high capacity of 422 mAh g^{-1} could be still obtained with an extremely high current density of 1600 mA g^{-1}. The hierarchical hollow structure Mn_2O_3 materials resulted in flexibility for volume change, and thus ensured a structural stability during charge−discharge cycling. Moreover, the XANES studies have revealed, for the first time, the conversion reaction process and the origin of capacity fading of the Mn_2O_3 electrodes.

2. EXPERIMENTAL SECTION

2.1. Materials Synthesis. The porous hierarchical Mn_2O_3 hollow microspheres were synthesized through annealing Mn-ethylene glycol (EG) precursors under air atmosphere at 750 °C for 10 h. Next, 0.6 g of manganese acetate tetrahydrate and 0.1 g of polyvinylpyrrolidone (PVP K-30) were mixed with 75 mL of EG. The as-obtained mixture was stirred for 30 min and then transferred into a 100 mL Teflon liner. The autoclave was sealed and maintained at 180 °C for 24 h, and finally cooled down to room temperature. The precipitate was collected by filtration, washed alternately with ethanol five times, and dried in a vacuum oven at 80 °C for 10 h. The precursors were further annealed at 750 °C for 10 h in air with a temperature changing rate of 5 °C min^{-1} to yield the final products. The synthesis of Mn_2O_3 microsheets were under the same experiment conditions as those mentioned above but without PVP K-30.

2.2. Materials Characterization. The phase purity and crystalline structure of the as-synthesized Mn_2O_3 material was identified by powder X-ray diffraction (Philips X'Pert Pro Super X-ray diffractometer, Cu Kα, radiation operating at 40 kV × 40 mA). Morphology of Mn_2O_3 microspheres was investigated by scanning electron microscopy (SEM, HITACHI S-4800). Transmission electron microscopy (TEM, FEI Tecnai-F30FEG) was used to analyze the structure of the Mn_2O_3 sample. The nitrogen adsorption/desorption isotherms were measured with a Micromeritics Tristar 3000 system, and the specific surface area was calculated by the Brunauer−Emmett−Teller (BET) method. Fourier transform infrared (FT-IR) analysis was carried out using pressed KBr disks in the range 4000−400 cm^{-1} using a Nicolet 330 spectrometer. Ex situ measurements of X-ray absorption fine structure (XAFS) were carried out at the beamline (BL14W1) at the Shanghai Synchrotron Radiation Facility (SSRF). In the Ar filled glovebox, thin-film Mn_2O_3 electrodes at different cutoff voltage and cycling numbers were obtained by disassembling the cells and washing with dimethyl carbonate (DMC), and then the electrodes were reassembled back into 2025 coin cells on which a hole of 2 mm in diameter was drilled for the XAFS studies.

2.3. Electrochemical Measurements. Mn_2O_3, carbon (acetylene black), and the binder of LA-133 (14.96 wt %) were mixed with a weight ratio of 70:20:10 in deionized water. The obtained slurry was pasted on Cu foil and dried in a vacuum oven at 100 °C overnight. The average weight of the working electrode materials was approximately 3 mg cm^{-2}. The electrochemical performances of Mn_2O_3 electrodes were evaluated using CR2025 coin cells assembled in a glovebox filled with argon. The coin cell consisted of a working electrode, Li metal foil as both counter electrode and reference electrode, a Celgard 2400 separator, a liquid electrolyte mixture (TINCI, Guangzhou) that contains 1 mol L^{-1} $LiPF_6$, and a solvent mixture of EC/DEC/DMC in a volume ratio of 1:1:1 with 2 wt % vinylene carbonate (VC) as additive. The cyclic voltammetry (CV) profiles were recorded with a electrochemical workstation (PARSTAT2263) at a scan rate of 0.1 mV s^{-1} in a potential window of 0.01−3.0 V. Electrochemical impedance spectroscopy (EIS) measurements were carried out on an electrochemical workstation (PARSTAT2263). Galvanostatic discharge/charge tests were conducted using a Land-CT2001A battery cycler (Wuhan, China) at room temperature.

3. RESULTS AND DISCUSSION

3.1. Structure and Morphology Characterization. In the synthesis process of adding PVP K-30, the hierarchical microspheres of Mn-EG precursors were first prepared and confirmed by XRD and IR characterization (Supporting Information Figure S1).[15,37] The hierarchical Mn_2O_3 hollow microspheres were obtained after the calcination of Mn-EG precursors. The XRD spectra of as-prepared Mn_2O_3 are shown in Figure 1. All the diffraction peaks can be perfectly indexed to the cubic bixbyite α-Mn_2O_3 (JCPDS, No. 41-1442). No peaks corresponding to other phases are found, confirming the high purity of the synthesized sample.

The SEM image in Figure 2 reveals that the resulting Mn_2O_3 hierarchical hollow microspheres are constituted of porous microsheets (Figure 2e). The diameter of the Mn_2O_3 microspheres is 6−10 μm, which is in accordance with the size of the commercial LIBs materials. And the Mn_2O_3 microspheres have a same size as that of the Mn-EG precursors (Figure 2b), but present a porous structure after calcination. The thickness of the porous microsheets is measured as 100 nm (Figure 2f), which is about 80 nm thicker than the Mn-EG precursors due to agglomeration of neighboring microsheets of Mn-EG precursors in calcination process (Figure 2c). However,

DOI: 10.1021/am509198k
ACS Appl. Mater. Interfaces 2015, 7, 8488−8494

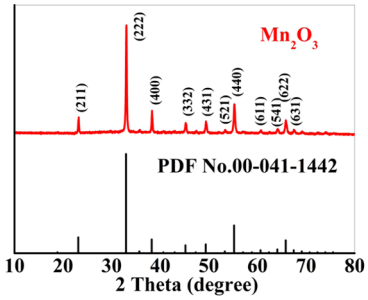

Figure 1. XRD patterns of Mn_2O_3 JCPDS standard (card number 42-0580) and Mn_2O_3 prepared by solvent-thermal method.

the product without adding PVP K-30 in the synthesis process presents microsheets structure shown in Figure S2. The specific surface area of the as-prepared Mn_2O_3 hierarchical hollow microspheres was measured at 7.83 m^2 g^{-1} by BET using N_2 absorption (Figure S3).

Figure 3 depicts the detailed structural features of Mn_2O_3 microspheres. From TEM and HRTEM images, we observe clearly hollow structure and atomic lattice of the Mn_2O_3. The hollow construction features illustrated in Figure 3a may ensure that the Mn_2O_3 microspheres can mitigate the local volume variation during charge−discharge cycling. It is interesting to see from Figure 3b that the particles are closely linked to form the porous microsheets, which is electric conductive and guarantees the structural stability in conversion reaction. High-resolution TEM (HRTEM) image displayed in Figure 3c indicates the lattice fringe with an interplanar distance of ca. 2.68 Å, corresponding to the (222) plane of cubic Mn_2O_3.

3.2. Electrochemical Performances of the Mn_2O_3 Hierarchical Hollow Microspheres. The electrochemical performances of the as-synthesized Mn_2O_3 were investigated by cyclic voltammetry (CV) and charge−discharge cycling (Figure 4). CV curves of the first three cycles of the Mn_2O_3 electrode are shown in Figure 4a. Two reductive peaks located at 1.1 and 0.2 V are clearly observed in the first cathodic process. The broad peak at about 1.1 V can be ascribed to the reduction of Mn^{3+} to Mn^{2+} and an irreversible reaction related to the formation of SEI layer.[32] The reduction action of Mn^{2+} to metallic Mn occurs near 0.2 V. However, only one peak is observed at 1.2 V in the first anodic process, indicating the lithium ion extraction reaction of Li_2O phase.[16,30,38] After the first cycle, nevertheless, only one cathodic peak at about 0.25 V and one anodic peak at 1.2 V are observed.

Figure 4b presents the first two discharge−charge curves of the porous hierarchical Mn_2O_3 hollow microspheres electrode at a current density of 500 mA g^{-1}. The first discharge profile consists of a slope at about 1.2 V and a wide plateau near 0.2 V, which consume an overall capacity of 1210 mAh g^{-1}. In the first charge curves, a wide slope appears at 1.2 V and the capacity is 760 mAh g^{-1} with a Coulombic efficiency of about 62.8%. The discharge plateau is shifted to about 0.5 V in the second cycle, and no change for charge plateau.

Figure 4c and d demonstrates the cycling performance and rate capability of the Mn_2O_3 electrode in galvanostatic experiments. A reversible capacity of 580 mAh g^{-1} at 500 mA g^{-1} with a high Coulombic efficiency about 99.7% was measured after 140 cycles (Figure 4c), maintaining higher capacity and retention rate than Mn_2O_3 microsheets (Figure S4). To evaluate the rate capability, the Mn_2O_3 electrode was charge−discharged at different rates. As illustrated in Figure 4d, reversible charge capacities of 751, 611, 511, and 422 mAh g^{-1} were measured respectively at 100, 400, 800, and 1600 mA g^{-1}. Compared to the data reported recently,[32,33] our Mn_2O_3 microspheres possess excellent electrochemical performance, which is attributed to (a) the porous hollow structural character ensuring the structure stability during conversion reaction cycling, (b) the hierarchical structure making each nanosheet contact directly with electrolyte, and (c) the pores between Mn_2O_3 nanoparticles allowing the fast diffusion of Li^+. In addition, the Mn_2O_3/carbon/LA133 electrodes after 140 cycles at 500 mA g^{-1} on copper foil were characterized by SEM as shown in Figure S5. Some of the porous and hierarchical structure still is preserved after such a long cycling process, indicating high structure stability.

3.3. XANES Study of Conversion Reaction Mechanism of Mn_2O_3 Electrode Materials. The XANES spectra of reference compounds of Mn, MnO, Mn_3O_4, and Mn_2O_3 (Figure S6) display an absorption Mn K-edge at 6539.0, 6544.2, 6547.0, and 6548.2 eV, respectively. The XANES spectra of the MnO, Mn_3O_4, and Mn_2O_3 exhibit a small pre-edge peak around 6539 eV. Due to the hybridization of the p

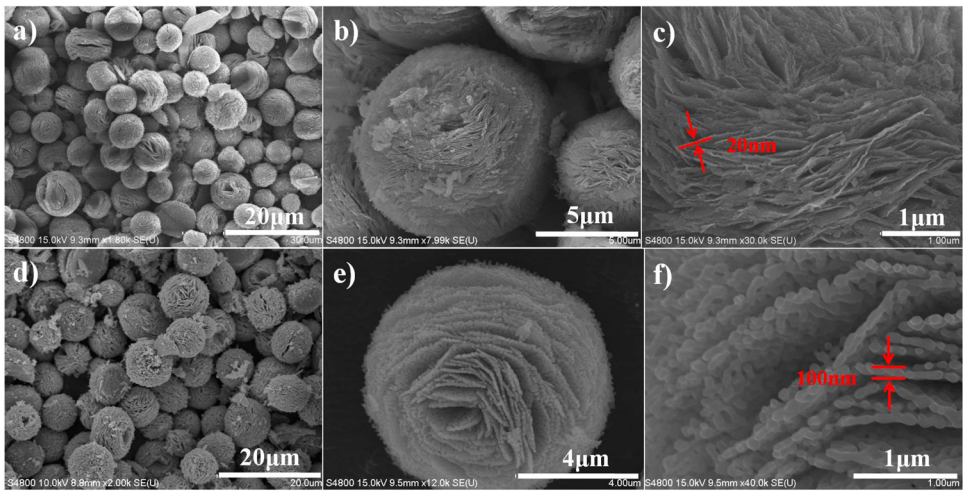

Figure 2. SEM images of Mn-ethylene glycol (EG) precursors (a, b, c) and the porous hierarchical Mn_2O_3 hollow microspheres (d, e, f) at different magnifications.

DOI: 10.1021/am509198k
ACS Appl. Mater. Interfaces 2015, 7, 8488−8494

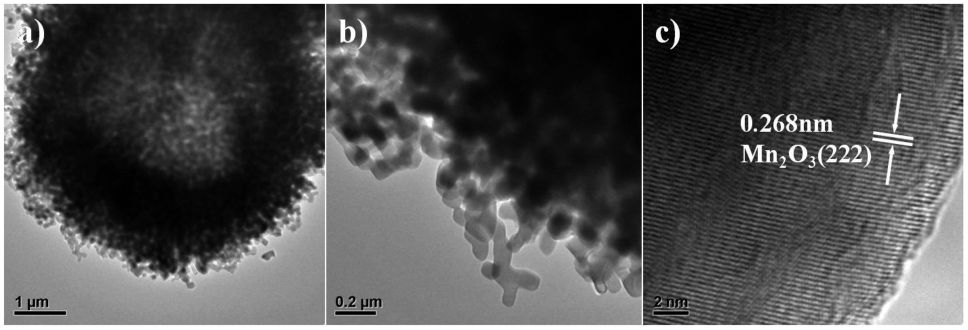

Figure 3. TEM (a, b) and HRTEM (c) images of the porous hierarchical Mn_2O_3 hollow microspheres.

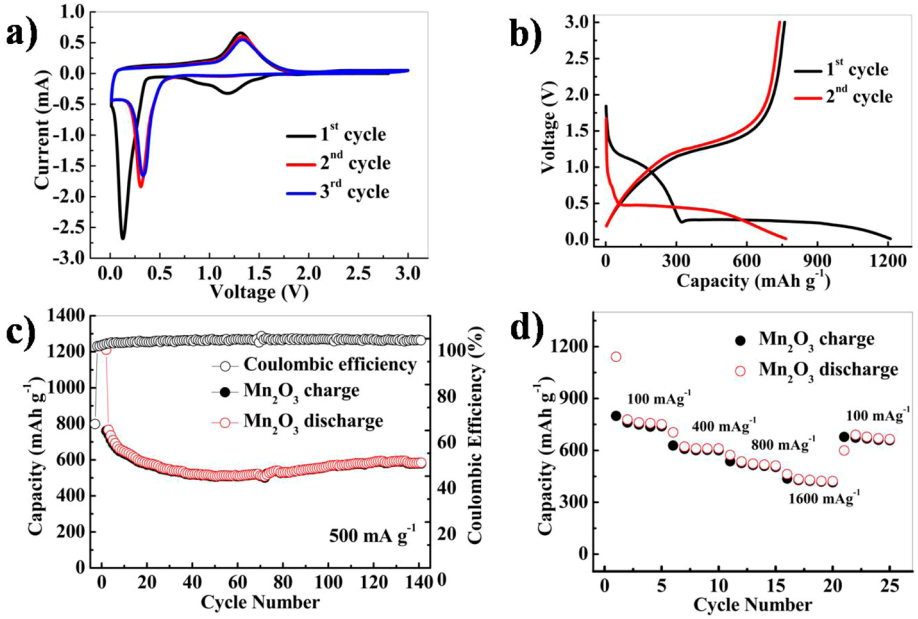

Figure 4. Electrochemical properties of the porous hierarchical Mn_2O_3 hollow microspheres anode: (a) first three consecutive CVs, (b) discharge−charge curves at a current of 500 mA g^{-1}, (c) cycling performance of the porous hierarchical Mn_2O_3 hollow microspheres at a current of 500 mA g^{-1}, and (d) rate capability of the porous hierarchical Mn_2O_3 hollow microspheres.

and d orbitals, the transition from 1s to 3d is normally forbidden, which is different from the case of the metallic Mn K-edge.[39]

The K-edge evolution of Mn element in the as-synthesized Mn_2O_3 microspheres in the first cycle was studied by ex situ XANES. As illustrated in Figure 5, when Mn_2O_3 is discharged to 1.5 V (Figure 5a), the E_0 (6548.2 eV) of the Mn K-edge is the same as that measured at open circuit potential (OCP), indicating no valence reduction in this stage, which is consistent with the electrochemical measurements. Compared to the reference compounds, the E_0 shifts to low energy and is the same as that of MnO when the Mn_2O_3 is discharged to 0.6 V, indicating that Mn^{3+} is reduced to Mn^{2+}. At the end of discharge process, the pre-edge peak disappears and the Mn K-edge position shifts to lower energy, illustrating a further reduction of the Mn^{2+} to Mn^0.

During the charge process, E_0 shifts to the inverse trend, which can be interpreted as an increase in the valence of the Mn (Figure 5b). When charged from 0.01 to 1.0 V, no obvious shift in the K-edge of Mn could be observed in comparison with that at 0.01 V, illustrating that the valence of Mn remains unchanged and the conversion reaction has not occurred. From 1.0 to 3 V in the charge process, the pre-edge peak reappears and the E_0 is the same as that of MnO. As illustrated in Figure 6, the E_0 at different states measured at characteristic points is shifted to low/high energy in discharge/charge processes, demonstrating clearly the valence evolution of Mn during the electrochemical conversion reaction processes.

To investigate the origin of the capacity loss of Mn_2O_3 materials during cycling, we analyzed the Mn K-edge XANES spectra of the Mn_2O_3 sample subjected to different cycling numbers (Figure 7). In the first charge/discharge cycle, the pristine Mn_2O_3 is reduced to metallic Mn when discharged to 0.01 V and oxidized to MnO while charged to 3.0 V. However, for the Mn_2O_3 samples subjected to 5, 10, and 50 cycles, the Mn K-edge energy shifts to low energy for the delithiated state (i.e., 6543.5, 6543.3, and 6543.6 eV, respectively) and keeps stable for the lithiated state (about 6539 eV). This indicates that the conversion reaction of metallic Mn and Li_2O phase to oxide (mainly MnO) is not a fully reversible reaction. As a consequence, the valence of Mn in the sample at charged state has decreased along with cycling, which leads to reduction of the amount of electrons involved in the reaction. As a result, the accumulation of Li_2O which does not participate in deconversion reaction makes the charge transfer resistance (R_{ct}) increase (Figure S7) and the capacity decay.

DOI: 10.1021/am509198k
ACS Appl. Mater. Interfaces 2015, 7, 8488−8494

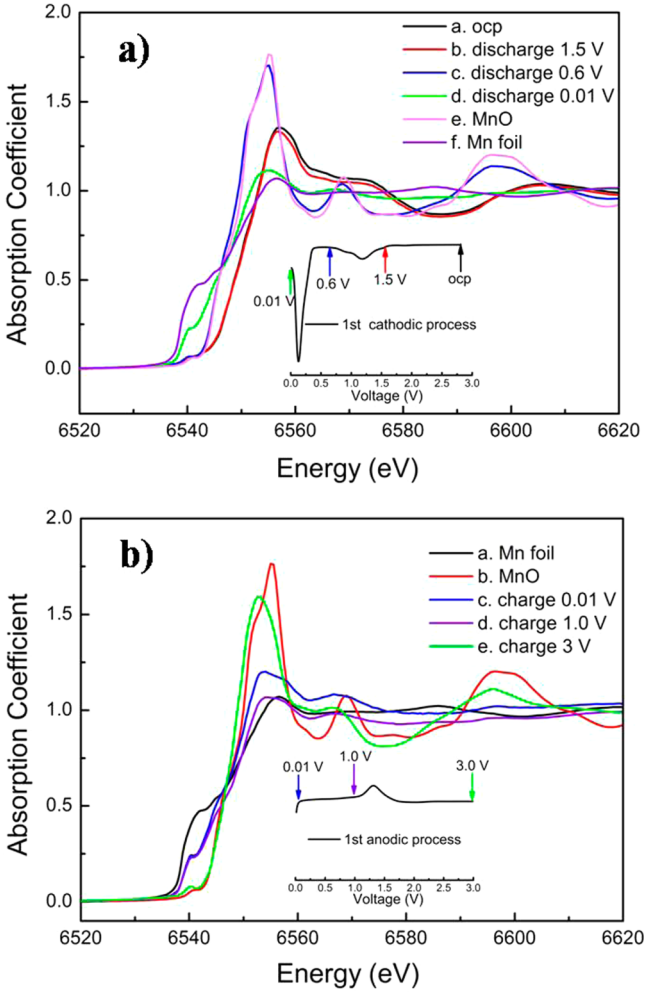

Figure 5. Ex situ Mn K-edge XANES spectra of Mn_2O_3 electrode at different preset voltages during the first discharging (a)/charging (b) process and Mn K-edge XANES spectra of Mn, MnO, and Mn_3O_4.

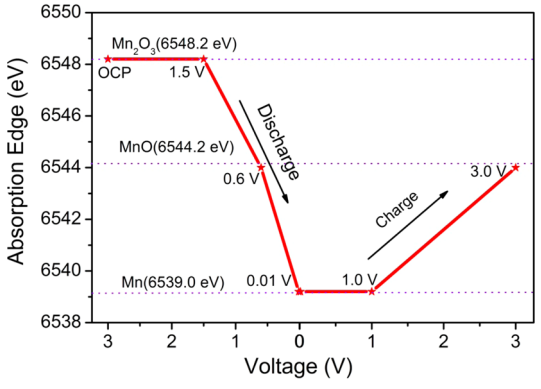

Figure 6. E_0 evolution of the Mn K-edge along with voltage change during the first discharge and charge processes.

From above ex situ XANES results, the conversion reaction processes of Mn_2O_3 electrodes may be suggested as follows. During the first discharge, the slope from 1.5 to 0.7 V may associate with the reduction of Mn^{3+} to Mn^{2+}, as expressed by eq 1 below. Then, a broad plateau appears at about 0.2 V, indicating the reduction action of Mn^{2+} to metallic Mn, as expressed by eq 2. From the first charge process, the

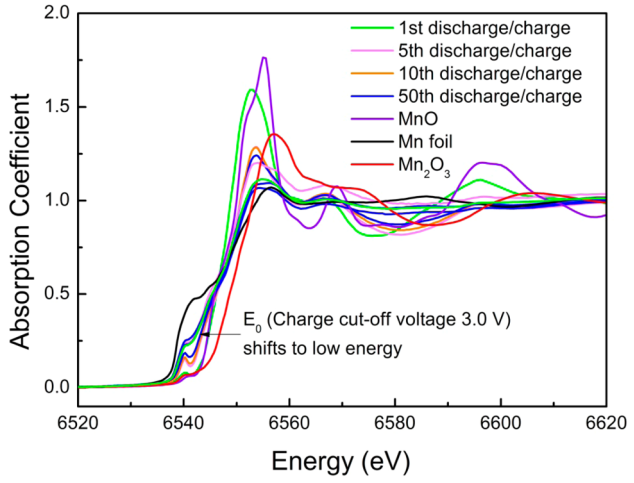

Figure 7. Ex situ Mn K-edge XANES spectra of different cyclic numbers Mn_2O_3 electrodes and Mn K-edge XANES spectra of Mn and MnO.

electrochemical reversible reaction undergoes the conversion between Mn and MnO_x, corresponding to eq 3.

$$2Li^+ + Mn_2O_3 + 2e^- \rightarrow 2MnO + Li_2O \quad (1)$$

$$2Li^+ + MnO + 2e^- \rightarrow Mn + Li_2O \quad (2)$$

$$Mn + xLi_2O \leftrightarrow MnO_x\ (0 < x < 1) + 2xLi^+ + 2xe^- \quad (3)$$

4. CONCLUSION

In the current study, a solvent-thermal method was used to synthesize porous hierarchical Mn_2O_3 hollow microspheres, which served as anode materials for the lithium ion battery. These special structural features of Mn_2O_3 guarantee its excellent electrochemical performance during charge/discharge processes. The hierarchical structure can ensure every subunit contacting with the electrolyte adequately, the pores between nanoparticles can facilitate both Li^+ and electron diffusion, and the hollow structure can mitigate efficiently the local volume variation. The as-synthesized porous hierarchical Mn_2O_3 hollow microspheres anode can deliver a reversible capacity of 580 mAh g^{-1} at a current density of 500 mA g^{-1} with a high coulombic efficiency about 99.7% after 140 cycles of charge−discharge. At high current densities of charge−discharge of 100, 400, 800, and 1600 mA g^{-1}, the Mn_2O_3 electrodes can still deliver reversible charge capacities of 751, 611, 511, and 422 mAh g^{-1}, respectively. The XANES spectra were used to characterize the Mn K-edge, and the results demonstrate that the Mn_2O_3 is reduced to metallic Mn when discharged to 0.01 V and oxidized to Mn^{2+} while charged to 3 V in the first cycle. In the subsequent cycles of charge−discharge, the average valence of Mn in the sample at charged state decreases, resulting from reducing the amount of electrons participating in the reaction, which is the origin of the irreversible capacity loss of Mn_2O_3 materials.

■ ASSOCIATED CONTENT

Supporting Information

XRD pattern and FT-IR spectrum of the Mn-EG, SEM images of the Mn_2O_3 microsheets without PVP K-30 in the synthesis process, N_2 adsorption/desorption measurements of the porous

DOI: 10.1021/am509198k
ACS Appl. Mater. Interfaces 2015, 7, 8488−8494

hierarchical Mn_2O_3 hollow microspheres, cycling performance of the Mn_2O_3 microsheets at a current of 500 mA g^{-1} in a potential window of 0.01−3.0 V, SEM images of the Mn_2O_3/carbon/LA 133 electrodes after 140 cycles at 500 mA g^{-1} on copper foil, reference compounds' Mn K-edge X-ray absorption near-edge structure (XANES), and EIS spectra of different cyclic numbers Mn_2O_3 electrodes. This material is available free of charge via the Internet at http://pubs.acs.org/.

AUTHOR INFORMATION

Corresponding Author

*E-mail: sgsun@xmu.edu.cn.

Notes

The authors declare no competing financial interest.

ACKNOWLEDGMENTS

This work was financially supported by NSFC (Grant Nos. 21373008, 21321062, and 21273184).

REFERENCES

(1) Armand, M.; Tarascon, J. M. Building Better Batteries. *Nature* **2008**, *451*, 652−657.

(2) Tarascon, J. M.; Armand, M. Issues and Challenges Facing Rechargeable Lithium Batteries. *Nature* **2001**, *414*, 359−367.

(3) Gu, X.; Chen, L.; Ju, Z. C.; Xu, H. Y.; Yang, J.; Qian, Y. T. Controlled Growth of Porous alpha-Fe_2O_3 Branches on beta-MnO2 Nanorods for Excellent Performance in Lithium-Ion Batteries. *Adv. Funct. Mater.* **2013**, *23*, 4049−4056.

(4) He, C. N.; Wu, S.; Zhao, N. Q.; Shi, C. S.; Liu, E. Z.; Li, J. J. Carbon-Encapsulated Fe_3O_4 Nanoparticles as a High-Rate Lithium Ion Battery Anode Material. *ACS Nano* **2013**, *7*, 4459−4469.

(5) Wang, X.; Wu, X. L.; Guo, Y. G.; Zhong, Y. T.; Cao, X. Q.; Ma, Y.; Yao, J. N. Synthesis and Lithium Storage Properties of Co_3O_4 Nanosheet-Assembled Multishelled Hollow Spheres. *Adv. Funct. Mater.* **2010**, *20*, 1680−1686.

(6) Xiao, X. L.; Liu, X. F.; Zhao, H.; Chen, D. F.; Liu, F. Z.; Xiang, J. H.; Hu, Z. B.; Li, Y. D. Facile Shape Control of Co_3O_4 and the Effect of the Crystal Plane on Electrochemical Performance. *Adv. Mater.* **2012**, *24*, 5762−5766.

(7) Yan, N.; Hu, L.; Li, Y.; Wang, Y.; Zhong, H.; Hu, X. Y.; Kong, X. K.; Chen, Q. W. Co_3O_4 Nanocages for High-Performance Anode Material in Lithium-Ion Batteries. *J. Phys. Chem. C* **2012**, *116*, 7227−7235.

(8) Needham, S. A.; Wang, G. X.; Liu, H. K. Synthesis of NiO Nanotubes for Use as Negative Electrodes in Lithium Ion Batteries. *J. Power Sources* **2006**, *159*, 254−257.

(9) Nam, I.; Kim, N. D.; Kim, G. P.; Park, J.; Yi, J. One Step Preparation of Mn3O4/Graphene Composites for Yse as An Anode in Li Ion Batteries. *J. Power Sources* **2013**, *244*, 56−62.

(10) Sun, Y. M.; Hu, X. L.; Luo, W.; Xia, F. F.; Huang, Y. H. Reconstruction of Conformal Nanoscale MnO on Graphene as A High-Capacity and Long-Life Anode Material for Lithium Ion Batteries. *Adv. Funct. Mater.* **2013**, *23*, 2436−2444.

(11) Xia, Y.; Xiao, Z.; Dou, X.; Huang, H.; Lu, X. H.; Yan, R. J.; Gan, Y. P.; Zhu, W. J.; Tu, J. P.; Zhang, W. K.; Tao, X. Y. Green and Facile Fabrication of Hollow Porous MnO/C Microspheres from Microalgaes for Lithium-Ion Batteries. *ACS Nano* **2013**, *7*, 7083−7092.

(12) Goodenough, J. B.; Kim, Y. Challenges for Rechargeable Li Batteries. *Chem. Mater.* **2010**, *22*, 587−603.

(13) Jiang, J.; Li, Y. Y.; Liu, J. P.; Huang, X. T.; Yuan, C. Z.; Lou, X. W. Recent Advances in Metal Oxide-based Electrode Architecture Design for Electrochemical Energy Storage. *Adv. Mater.* **2012**, *24*, 5166−5180.

(14) Li, X. W.; Xiong, S. L.; Li, J. F.; Liang, X.; Wang, J. Z.; Bai, J.; Qian, Y. T. MnO@Carbon Core-Shell Nanowires as Stable High-Performance Anodes for Lithium-Ion Batteries. *Chem.—Eur. J.* **2013**, *19*, 11310−11319.

(15) Hu, L.; Sun, Y. K.; Zhang, F. P.; Chen, Q. W. Facile Synthesis of Porous Mn_2O_3 Hierarchical Microspheres for Lithium Battery Anode with Improved Lithium Storage Properties. *J. Alloys Compd.* **2013**, *576*, 86−92.

(16) Chen, S. L.; Liu, F.; Xiang, Q. J.; Feng, X. H.; Qiu, G. H. Synthesis of Mn_2O_3 Microstructures and Their Energy Storage Ability Studies. *Electrochim. Acta* **2013**, *106*, 360−371.

(17) Haag, J. M.; Pattanaik, G.; Durstock, M. F. Nanostructured 3D Electrode Architectures for High-Rate Li-Ion Batteries. *Adv. Mater.* **2013**, *25*, 3238−3243.

(18) Yu, L.; Zhang, L.; Bin Wu, H.; Zhang, G. Q.; Lou, X. W. Controlled Synthesis of Hierarchical $Co_xMn_{3-x}O_4$ Array Micro-/Nanostructures with Tunable Morphology and Composition as Integrated Electrodes for Lithium-Ion Batteries. *Energy Environ. Sci.* **2013**, *6*, 2664−2671.

(19) Banerjee, A.; Singh, U.; Aravindan, V.; Srinivasan, M.; Ogale, S. Synthesis of CuO Nanostructures from Cu-Based Metal Organic Framework (MOE-199) for Application as Anode for Li-Ion Batteries. *Nano Energy* **2013**, *2*, 1158−1163.

(20) Kasavajjula, U.; Wang, C. S.; Appleby, A. J. Nano- and Bulk-Silicon-Based Insertion Anodes for Lithium-Ion Secondary Cells. *J. Power Sources* **2007**, *163*, 1003−1039.

(21) Guo, Y. G.; Hu, J. S.; Wan, L. J. Nanostructured Materials for Electrochemical Energy Conversion and Storage Devices. *Adv. Mater.* **2008**, *20*, 2878−2887.

(22) Yin, Y. X.; Xin, S.; Guo, Y. G. Nanoparticles Engineering for Lithium-Ion Batteries. *Part. Part. Syst. Charact.* **2013**, *30*, 737−753.

(23) Xiao, J.; Zheng, J. M.; Li, X. L.; Shao, Y. Y.; Zhang, J. G. Hierarchically Structured Materials for Lithium Batteries. *Nanotechnology* **2013**, *24*, 424004.

(24) Zhang, B.; Zhang, Y. B.; Miao, Z. Z.; Wu, T. X.; Zhang, Z. D.; Yang, X. G. Micro/Nano-Structure Co_3O_4 as High Capacity Anode Materials for Lithium-Ion Batteries and the Effect of the Void Volume on Electrochemical Performance. *J. Power Sources* **2014**, *248*, 289−295.

(25) Zhong, H. X.; Zhou, P.; Yue, L.; Tang, D. P.; Zhang, L. Z. Micro/Nano-Structured SnS_2 Negative Electrodes Using Chitosan Derivatives as Water-Soluble Binders for Li-Ion Batteries. *J. Appl. Electrochem.* **2014**, *44*, 45−51.

(26) Lai, X. Y.; Halpert, J. E.; Wang, D. Recent Advances in Micro-/Nano-Structured Hollow Spheres for Energy Applications: From Simple to Complex Systems. *Energy Environ. Sci.* **2012**, *5*, 5604−5618.

(27) Shen, J. Y.; Wang, H.; Zhou, Y.; Ye, N. Q.; Wang, L. J. Continuous Hollow TiO_2 Structures with Three-Dimensional Interconnected Single Crystals and Large Pore Mesoporous Shells for High-Performance Lithium-Ion Batteries. *CrystEngComm* **2012**, *14*, 6215−6220.

(28) Wang, Z.; Zhou, L.; Lou, X. W. Metal Oxide Hollow Nanostructures for Lithium-Ion Batteries. *Adv. Mater.* **2012**, *24*, 1903−1911.

(29) Zhang, G. Q.; Wu, H. B.; Hoster, H. E.; Lou, X. W. Strongly Coupled Carbon Nanofiber-Metal Oxide Coaxial Nanocables with Enhanced Lithium Storage Properties. *Energy Environ. Sci.* **2014**, *7*, 302−305.

(30) Qiu, Y. C.; Xu, G. L.; Yan, K. Y.; Sun, H.; Xiao, J. W.; Yang, S. H.; Sun, S. G.; Jin, L. M.; Deng, H. Morphology-Conserved Transformation: Synthesis of Hierarchical Mesoporous Nanostructures of Mn_2O_3 and the Nanostructural Effects on Li-Ion Insertion/Deinsertion Properties. *J. Mater. Chem.* **2011**, *21*, 6346−6353.

(31) Wang, J. F.; Zhu, G.; Deng, L. J.; Kang, L. P.; Hao, Z. P.; Liu, Z. H. Novel Synthesis and Formation Process of Uniform Mn_2O_3 Cubes. *CrystEngComm* **2012**, *14*, 8253−8260.

(32) Li, Q.; Yin, L.; Li, Z.; Wang, X.; Qi, Y.; Ma, J. Copper Doped Hollow Structured Manganese Oxide Mesocrystals with Controlled Phase Structure and Morphology as Anode Materials for Lithium Ion Battery with Improved Electrochemical Performance. *ACS Appl. Mater. Interfaces* **2013**, *5*, 10975−10984.

(33) Zhang, X.; Qian, Y. T.; Zhu, Y. C.; Tang, K. B. Synthesis of Mn_2O_3 Nanomaterials with Controllable Porosity and Thickness for

DOI: 10.1021/am509198k
ACS Appl. Mater. Interfaces 2015, 7, 8488−8494

Enhanced Lithium-Ion Batteries Performance. *Nanoscale* **2014**, *6*, 1725−1731.
(34) Deng, Y. F.; Li, Z. N.; Shi, Z. C.; Xu, H.; Peng, F.; Chen, G. H. Porous Mn_2O_3 Microsphere as A Superior Anode Material for Lithium Ion Batteries. *RSC Adv.* **2012**, *2*, 4645−4647.
(35) Lv, D. P.; Bai, J. Y.; Zhang, P.; Wu, S. Q.; Li, Y. X.; Wen, W.; Jiang, Z.; Mi, J. X.; Zhu, Z. Z.; Yang, Y. Understanding the High Capacity of Li_2FeSiO_4: In Situ XRD/XANES Study Combined with First-Principles Calculations. *Chem. Mater.* **2013**, *25*, 2014−2020.
(36) Zhong, K. F.; Zhang, B.; Luo, S. H.; Wen, W.; Li, H.; Huang, X. J.; Chen, L. Q. Investigation on Porous MnO Microsphere Anode for Lithium Ion Batteries. *J. Power Sources* **2011**, *196*, 6802−6808.
(37) Hu, L.; Zhong, H.; Zheng, X. R.; Huang, Y. M.; Zhang, P.; Chen, Q. W. $CoMn_2O_4$ Spinel Hierarchical Microspheres Assembled with Porous Nanosheets as Stable Anodes for Lithium-Ion Batteries. *Sci. Rep.* **2012**, *2*, 986−993.
(38) Chang, L.; Mai, L. Q.; Xu, X.; An, Q. Y.; Zhao, Y. L.; Wang, D. D.; Feng, X. Pore-Controlled Synthesis of Mn_2O_3Microspheres for Ultralong-Life Lithium Storage Electrode. *RSC Adv.* **2013**, *3*, 1947−1952.
(39) Ma, S. B.; Nam, K. W.; Yoon, W. S.; Yang, X. Q.; Ahn, K. Y.; Oh, K. H.; Kim, K. B. Electrochemical Properties of Manganese Oxide Coated onto Carbon Nanotubes for Energy-Storage Applications. *J. Power Sources* **2008**, *178*, 483−489.

DOI: 10.1021/am509198k
ACS Appl. Mater. Interfaces 2015, 7, 8488−8494